Cooperative Down-Conversion Luminescence in Tb^{3+}/Yb^{3+} Co-Doped $LiYF_4$ Single Crystals

Li Fu,[1] Haiping Xia,[1] Yanmin Dong,[1] Shanshan Li,[1] Haochuan Jiang,[2] and Baojiu Chen[3]

[1]Key Laboratory of Photo-Electronic Materials, Ningbo University, Ningbo 315211, China
[2]Ningbo Institute of Materials Technology and Engineering, Chinese Academy of Sciences, Ningbo 315201, China
[3]Department of Physics, Dalian Maritime University, Dalian 116026, China

DOI: 10.1109/JPHOT.2014.2300495

Manuscript received November 5, 2013; revised January 4, 2014; accepted January 6, 2014. Date of publication January 16, 2014; date of current version January 23, 2014. This work was supported in part by the National Natural Science Foundation of China under Grants 51272109, 50972061, and 50972021; by the Natural Science Foundation of Zhejiang Province under Grant R4100364; by the Natural Science Foundation of Ningbo City under Grant 2012A610115; and by the K. C. Wong Magna Fund in Ningbo University. Corresponding author: H. Xia (e-mail: hpxcm@nbu.edu.cn).

Abstract: Cooperative down-conversion (DC) with emission of two near-infrared photons for each blue photon absorbed was achieved in Tb^{3+}/Yb^{3+} co-doped yttrium lithium fluoride single crystals grown by an improved Bridgman method. The luminescent properties of the crystals were investigated through photoluminescence excitation, emission spectra, and decay curves. With the excitation of Tb^{3+} ion by a 486 nm light, emission between 980 and 1030 nm from the Yb^{3+} : $^2F_{5/2} \rightarrow {}^2F_{7/2}$ transition was observed, and this emission originated from the DC between Tb^{3+} and Yb^{3+} ions. The energy transfer processes are studied based on the Inokuti–Hirayama's model, and the interaction between Tb^{3+} and Yb^{3+} is confirmed to be electric dipole–dipole. The large quantum cutting efficiency approaches up to 166.7% for 0.32 mol% of Tb^{3+} and 7.98 mol% of Yb^{3+} co-doped $LiYF_4$, which is potentially used as a DC layer in silicon-based solar cells.

Index Terms: Tb^{3+}, Yb^{3+}, $LiYF_4$ single crystal, down-conversion, energy transfer, I-H model.

1. Introduction

Nowadays there is a great interest in solar power due to its green, abundance and renewability [1]. The capacity to convert sunlight into electricity by photovoltaic silicon solar cell is a major issue of human using solar energy to solve the energy problem [2], [3] at the present time. However, energy conversion rate of crystal silicon solar cell in the market is mostly about 15%, which is far lower than 29% by classical theory. This difference is due to the spectral mismatch that results in the major part of the energy losses in solar cells. In order to increase the conversion efficiency of concentrated sunlight to electricity, there are two different ways to be considered. One is using the Multi-junction tandem cell III-V solar cells [4]. Recent works on InGaAsN-containing quantum wells grown on GaAs have led to high performance and very low threshold lasers [5]–[8], and these advances in dilute-nitride materials had led to recent promising results with more than 43.5% solar conversion efficiency [9]. The other is using spectral modification [2], [10].The main methods of spectral modification include up-conversion, photoluminescence and down-conversion (DC) [11].

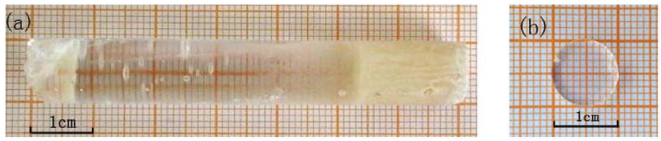

Fig. 1. Tb^{3+}/Yb^{3+} co-doped $LiYF_4$ single crystal. (a) As grown crystal. (b) Polished crystal.

Recently, cooperative down-conversion has attracted much more attention for its potential applications in the fields of solar cells, plasma display *et al.* This method is based on the principle that two-energy near-infrared (NIR) photons were generated when each incident high-energy ultraviolet (UV) or visible (VIS) photon was absorbed. By such spectral modification, the energy conversion rate of crystal silicon solar cell can be enhanced significantly because the most effective absorption band of crystalline Si for sunlight is around near-infrared wavelength of 1000 nm.

DC has been realized from Tb^{3+}/Yb^{3+} [12]–[15], [21], Pr^{3+}/Yb^{3+} [15], [16], Tm^{3+}/Yb^{3+} [15], [17], Ce^{3+}/Yb^{3+} [18], [19], and Nd^{3+}/Yb^{3+} [20] couples codoped in micro-crystals or glasses in converting visible photons into near-infrared [12]–[20]. In previous investigations, most reported materials are in the forms of powders [12], [15], [18], [21] and glasses [13], [14], [16], [17], [19], [20]. Generally, powders have strong scattering and low transmission for lights [1], [22]. And some glasses have low optimum mechanical, thermal, chemical properties, and low luminescent efficiency for rare earth ions located in the glass network [23], [24]. They are deficient to be applied effectively in solar cells and other optical devices due to those drawbacks.

In fact, many single crystals exhibit better properties in high optical transmission and luminescent efficiency for solar cell applications [1]. However, there are too few reports on rare earth doped single crystals for DC. $LiYF_4$ crystal doped with rare-earth ions has been proven to be an efficient all-solid-state laser media because of its good chemical durability and thermal stability, high optical transparency in a wide wavelength range from infrared to ultraviolet, and lower phonon energy. These characteristics also render $LiYF_4$ single crystals as extremely suitable for QC. More Recently, we have presented experimental evidences for a cooperative energy transfer (ET) from Pr^{3+} to two Yb^{3+} ions in the Pr^{3+}/Yb^{3+} co-doped $LiYF_4$ single crystal for potential application in solar cells [1].

In the Tb^{3+}/Yb^{3+} system, the $^2F_{7/2} \rightarrow {}^2F_{5/2}$ single transition of Yb^{3+} is located at approximately half the energy of $Tb^{3+}: {}^5D_4 \rightarrow {}^7F_6$ transition and the emission of Yb^{3+} ions by $^2F_{5/2} \rightarrow {}^2F_{7/2}$ transition is located in the range between 950 and 1050 nm, which matches the energy gap of silicon well [15], [21]. The DC has been experimentally realized in the Tb^{3+}/Yb^{3+} codoped $Yb_\chi Y_{1-\chi}PO_4 : Tb^{3+}$ compounds [13], in which the theoretical maximum quantum efficiency can reach nearly 200%.

In this paper, we measured the fluorescence spectra of Tb^{3+}/Tb^{3+} co-doped in $LiYF_4$ single crystal prepared by a Bridgman method using a sealed platinum crucible in an air atmosphere. The cooperative ET from Tb^{3+} to Yb^{3+} ions in the Tb^{3+}/Yb^{3+} co-doped $LiYF_4$ single crystal will be discussed.

2. Experimental Details

The Tb^{3+}, Yb^{3+} singly and Tb^{3+}/Yb^{3+} doubly doped $LiYF_4$ single crystals were grown using an improved Bridgman method. Y^{3+} ions were substituted by Tb^{3+} and Yb^{3+} ions. In order to ensure crystallization of the desired phase, feed materials for crystal growth were prepared with a slight excess of LiF. The raw materials (LiF, YF_3, TbF_3, YbF_3 powders) with a 99.999% purity were weighed according to the formula $LiY_{1-\chi}Tb_\chi F_4$, $LiY_{1-\gamma}Yb_\gamma F_4$, and $LiY_{1-\chi-\gamma}Tb_\chi Yb_\gamma F_4$, respectively. The detailed process of the growth and schematic of the apparatus used for the Bridgman method have been reported in our previous works [25].

The grown Tb^{3+}/Yb^{3+} co-doped $LiYF_4$ single crystal with the $\langle 100 \rangle$ direction is shown in Fig. 1. It was light yellow and transparent. The color changed gradually along the growth direction. The top of

TABLE 1

Concentration of Tb^{3+} and Yb^{3+} ions in the crystals (mol%)

samples	a0	a1	a2	b0	b1	b2	b3
Tb^{3+}	1.05	0	1.05	0.32	0.32	0.33	0.32
Yb^{3+}	0	1.96	1.96	0	1.98	4.97	7.98

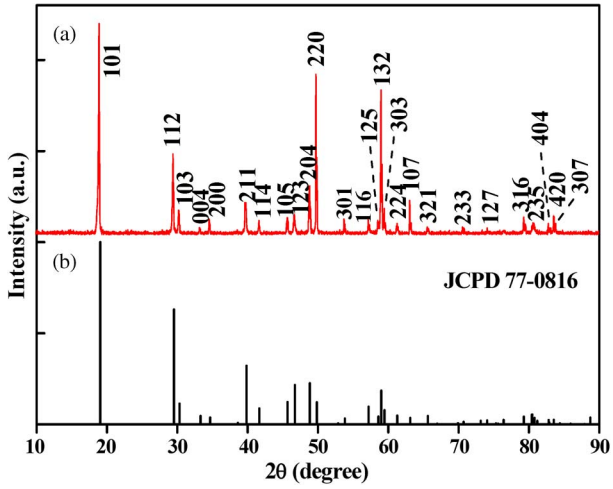

Fig. 2. (a) XRD pattern of the $LiYF_4$: Tb^{3+}/Yb^{3+}; (b) the standard line pattern of the orthorhombic phase $LiYF_4$ (JCPD 77-0816).

the crystals is opaque with a segregation layer comprised of redundant LiF and other impurities. The crystal was cut into small pieces and well polished on both sides to about 2 mm thickness for optical measurements.

The X-ray diffraction (XRD) was measured using a XD-98X diffractometer (XD-3, Beijing). The absorption spectra were recorded with a Cary 500 UV/VIS/NIR spectrophotometer (Agilent Co., America). The excitation and emission spectra and decay curves were obtained with a FLSP 920 type spectrometer (Edinburgh Co., England). The Tb^{3+} and Yb^{3+} concentrations in $LiYF_4$ single crystal Tb^{3+} and Yb^{3+} were measured by the inductive coupled plasma atomic emission spectroscopy (ICP-AES, PerkinElmer Inc., Optima 3000). All the measurements were performed at room temperature. Table 1 shows the concentrations of Tb^{3+} and Yb^{3+} in some samples.

3. Results and Discussion

The X-ray diffraction pattern for Tb^{3+}/Yb^{3+} co-doped $LiYF_4$ crystal is shown in Fig. 2(a). By comparing the peak positions with those in JCPD 77-8016 of $LiYF_4$ displayed in Fig. 2(b), one can confirm that the crystal is of pure orthorhombic phase and the current doping level do not cause any obvious peak shift or second phase. The similar XRD patterns are obtained from different Tb^{3+} and Yb^{3+} doping concentrations of this experiment, verifying that all of the samples have been crystallized into the pure orthorhombic phase.

The absorption spectra of samples a1, a2, and undoped $LiYF_4$ crystals at room temperature in the region of 300–1100 nm are shown in Fig. 3. No visible absorption bands were observed in undoped $LiYF_4$ crystal, and an obvious band at 980 nm attributed to Yb^{3+} : $^2F_{7/2} \rightarrow {}^2F_{5/2}$ in Yb^{3+} singly doped one was observed. However, an strong absorption band at 980 nm (Yb^{3+} :^{2} $F_{7/2} \rightarrow {}^2F_{5/2}$) and another one at 486 nm (Tb^{3+} :^{7} $F_6 \rightarrow {}^5$ D_4) were observed in Tb^{3+}/Yb^{3+} codoped crystal. It indicates

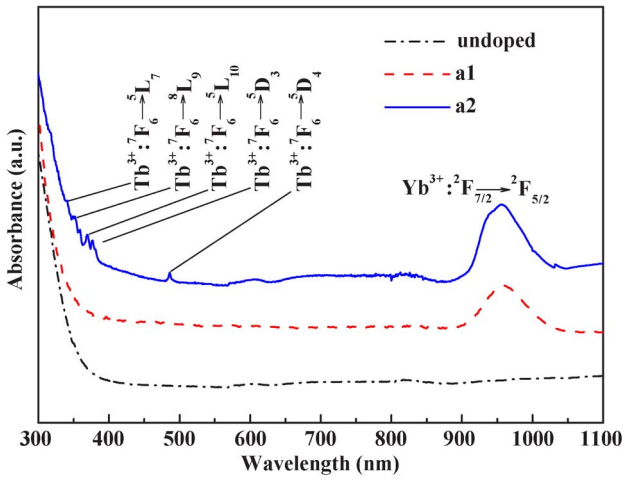

Fig. 3. Absorption spectra of the undoped (dash dot line), Yb^{3+} doped (dash line) and Tb^{3+}/Yb^{3+} co-doped $LiYF_4$ crystals (solid line).

that this crystal can be pumped efficiently by a 486 nm light. Meanwhile some bands centered at 340, 350, 365, 378 and 486 nm appeared and correspond to the energy level transitions of Tb^{3+} from $^7F_6$ to $^5L_j (j = 7, 8 \text{ and } 9)$, $^5D_3$ and $^5D_4$, respectively.

The excitation(a) and emission(b) spectra of samples a0, a1 and a2 are depicted in Fig. 4(a) and (b), respectively. Meanwhile, the energy level diagram of Tb^{3+} and Yb^{3+} in $LiYF_4$ crystals has also been shown in Fig. 4(c). An intense excitation band at 486 nm can be observed by monitoring emissions from both Tb^{3+} :^{5} $D_4 \rightarrow ^7$ F_5 transition at 544 nm and Yb^{3+} :^{2} $F_{5/2} \rightarrow ^2$ $F_{7/2}$ transition at 980 nm in Tb^{3+}/Yb^{3+} co-doped $LiYF_4$ crystal of sample a2 in Fig. 4(a). However, the band at 486 nm can be observed only by monitoring Tb^{3+} : $^5D_4 \rightarrow ^7F_5$ transition at 544 nm in Tb^{3+} singly doped crystal, and the absorption bands in Yb^{3+} singly doped crystal are very weak, as shown in Fig. 4(a). Three emission peaks in visible range at 544, 587 and 620 nm are observed in Tb^{3+} singly doped $LiYF_4$ crystal of sample a0 in Fig. 4(b) under the excitation of 486 nm light. They correspond to the transitions of $^5D_4 \rightarrow ^7$ $F_j (j = 5, 4 \text{ and } 3)$ [12]–[15], [21] as shown in Fig. 4(c). Multiple sharp peaks around those emission bands can be observed. These sharp peaks may be attributed to the energy splitting in crystal. It can also be found from Fig. 4(b) that the 544, 587 and 620 nm emission intensities decrease when Yb^{3+} ion is co-doped into Tb^{3+}-$LiYF_4$ crystal of sample a2, and an intense new emission peak around 1000 nm which is attributed to the transitions from the Stark level $^2F_{5/2}$ multiplet of Yb^{3+} to the Stark level $^2F_{7/2}$ multiplet appears. The emission around 1000 nm is very weak under excitation of 486 nm light for Yb^{3+} singly doped $LiYF_4$ of sample a1 in Fig. 4(b), and no absorption exists at 486 nm for Yb^{3+} singly doped $LiYF_4$ in Fig. 3. The above facts indicate that a possible ET from Tb^{3+} to Yb^{3+} exists in Tb^{3+}/Yb^{3+} codoped $LiYF_4$ crystal.

The possible mechanisms of the ET processes between Tb^{3+} and Yb^{3+} ions have been reported by Vergeer *et al.* [13]. In this paper, we attempt to quantitatively investigate the energy transfers between Tb^{3+} and Yb^{3+}. It can be seen from the energy level diagram of Fig. 4(c) that the $^5D_4$ level of Tb^{3+} is located just above twice the energy for $^2F_{5/2}$ of Yb^{3+}. One Tb^{3+} ion transfers its energy to two Yb^{3+} ions or radiates to the lower energy states associated with the emissions at 544, 587 and 620 nm which are assigned to the transition from $^5D_4$ to $^7F_j (j = 5, 4 \text{ and } 3)$ levels [12]–[15], [21], respectively, under irradiation at 486 nm. However, resonant ET from Tb^{3+} :^{5} D_4 state to one Yb^{3+} is not possible because the Yb^{3+} has only one excited state around 1000 nm and no transition from Tb^{3+} :^{5} D_4 is suitable to match the gap of Yb^{3+}. The mismatch between $^5D_4$ state of Tb^{3+} and $^2F_{5/2}$ state of Yb^{3+} is about 10372 cm^{-1} and the phonon energy in $LiYF_4$ crystal is about 425 cm^{-1} from our measured Raman spectrum in Tb^{3+}/Yb^{3+} codoped $LiYF_4$ crystal, which almost excludes the phonon assisted ET process. Then it is reasonable to propose a cooperative DC process from one Tb^{3+} ion to two Yb^{3+} ions to explain this ET process shown in Fig. 4(c). After excitation of

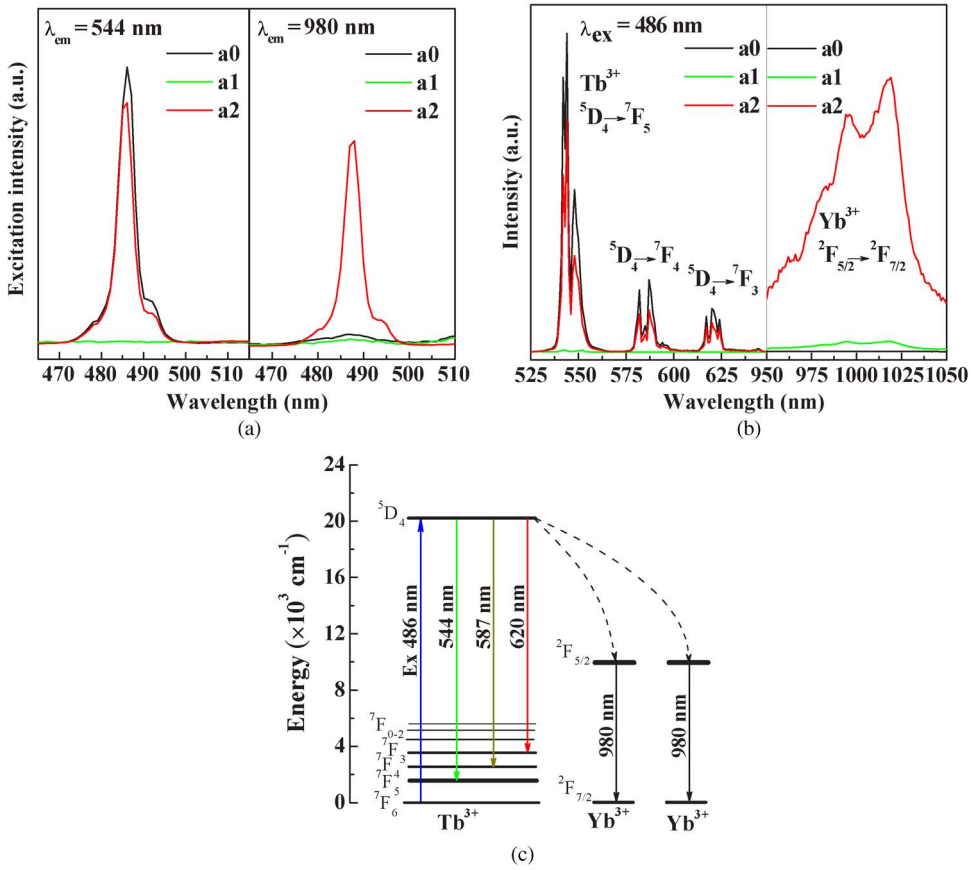

Fig. 4. (a) Excitation and (b) emission spectra of Tb^{3+} doped, Yb^{3+} doped and Tb^{3+}/Yb^{3+} co-doped $LiYF_4$ crystals. (c) Energy level diagram of Tb^{3+} and Yb^{3+} ions. The ET processes are indicated by dashed lines and excitation and emission transitions are indicated by solid lines.

Tb^{3+} :^{5} D_4 level by 486 nm, the de-excitation pathway of the ET process is cooperative down-conversion mechanism: $^5D_4(Tb^{3+}) \rightarrow {}^2F_{5/2}(Yb^{3+}) + {}^2F_{5/2}(Yb^{3+})$. Since the energy of a visible photon absorbed is more than twice that of a NIR photon emission of 980 nm, it is theoretically possible to achieve two NIR emission photons for every incident visible photon with quantum efficiency of up to 200%.

Fig. 5 presents the photoluminescence spectra for χmol% Tb^{3+}/γmol%Yb^{3+} samples upon light excitation at 486 nm corresponding to the Tb^{3+} :^{7} F_6 $\rightarrow$^{5} D_4 transition, where $\chi = 0.32, 0.32, 0.33, 0.32$, and $\gamma = 0, 1.98, 4.97$ and 7.98, respectively. The characteristics of emission bands are similar to those shown in Fig. 4(b). It can be seen from Fig. 5 that, when the Tb^{3+} concentration is held at about 0.32 mol%, the intensity of the green emission at 544 nm decreases and the NIR emission at 980–1030 nm increases monotonically as the Yb^{3+} concentration increases from 0 to 7.98 mol%. The NIR emission band at 980–1030 nm reaches a maximum when the Yb^{3+} concentration is $\sim$7.98 mol%. However, there is no emission in the NIR in the Tb^{3+} ion singly doped $LiYF_4$ sample.

The decay curves of the Tb^{3+} :^{5} D_4 $\rightarrow$^{7} F_5 luminescence at 544 nm for Tb^{3+}/Yb^{3+} codoped $LiYF_4$ samples under 486 nm light excitation are shown in Fig. 6. For 0 mol% Yb^{3+} concentration, the decay curve of 0.32 mol% (Tb^{3+}) singly doped $LiYF_4$ sample is close to single exponential with a lifetime of 4.68 ms. When the Yb^{3+} ions are introduced, energy transfer between Tb^{3+} and Yb^{3+} occurs. The decay lifetime decreases rapidly with the increase of Yb^{3+} ion from 0 mol% to 7.98 mol% in the co-doped samples, and the decay curves become non-exponential with the average lifetime

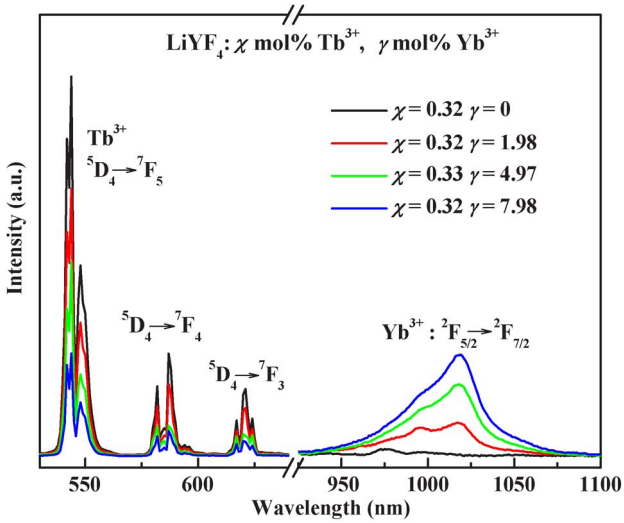

Fig. 5. Visible-NIR emission spectra of various Tb^{3+}/Yb^{3+} co-doped $LiYF_4$ crystals upon excitation of 486 nm.

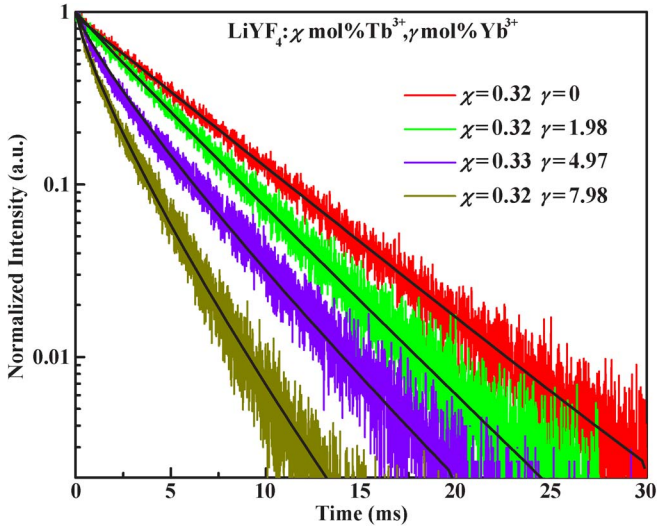

Fig. 6. Decay curves of the Tb^{3+}/Yb^{3+} ions co-doped $LiYF_4$ crystal samples surveyed at 544 nm under 486 nm excitation. The black solid lines are the stretched exponential fits for the decays.

decreasing from 4.68 ms to 1.56 ms. One can evaluate the average experimental lifetime for the non-exponential nature of the emission decay of these samples by the following equation [26]:

$$\tau_{avg} = \frac{\int I(t)tdt}{\int I(t)dt} \tag{1}$$

where $I(t)$ is the luminescence intensity as a function of time t. The results are listed in Table 2.

The stretched exponential function shown below is best to describe the decay curves in Fig. 6 [27]

$$I(t) = I_0 \exp\left((-t/\tau)^{\beta}\right) \qquad 0 < \beta < 1 \tag{2}$$

TABLE 2

Luminescence decay parameters, average decay lifetime, ETE and QE for χ mol% Tb^{3+} and γ mol% Yb^{3+} co-doped in $LiYF_4$ samples

(x, γ)	$\tau_{avg}(ms)$	$\tau\,(ms)$	β	$\tau_0(ms)$	$\eta_{ETE}(\%)$	$\eta_{QE}(\%)$
(1.05, 0)	4.72	5.13	1	…	…	…
(1.05, 1.96)	3.97	4.19	0.98	…	15.9	115.9
(0.32, 0)	4.68	4.96	1	…	…	…
(0.32, 1.98)	3.53	3.72	0.97	3.97	19.8	119.8
(0.33, 4.97)	2.49	2.33	0.85	2.75	46.8	146.8
(0.32, 7.98)	1.56	1.37	0.81	2.20	66.7	166.7

where $I(t)$ and I_0 represent the luminescence intensity during decay and at $t = 0$, respectively. The parameters τ and β depend on the material and other conditions such as temperature [28]. The parameter τ is a characteristic lifetime for the decay of Tb^{3+} excited states. And the parameter β, a dispersion factor ranging from 0 to 1, represents the degree to which the measured decay differs from a purely exponential decay. Fig. 6 displays the stretched exponential fit of the luminescence decay curves of various Tb^{3+}/Yb^{3+} doped samples. The obtained parameters τ and β are listed in Table 2. One can note that the parameter β was reduced with the increasing of Yb^{3+} concentration when the concentration of Tb^{3+} was held constant at $\sim$0.32 mol%. The lifetime τ is clearly decreased with increase of Yb^{3+} concentration in $LiYF_4$. It indicates the existence of ET from Tb^{3+} ions to Yb^{3+} ions in the samples.

It is well known that the non-exponential fluorescent decay follows the Inokuti–Hirayama's model [1], [17]. The fluorescent decay curves can then be expressed as

$$I(t) = I(0)\exp\left(-\frac{t}{\tau_0} - \frac{4\pi}{3}\Gamma\left(1-\frac{3}{s}\right)R_0^3 N\left(\frac{t}{\tau_0}\right)^{\frac{3}{s}}\right) \tag{3}$$

where $I(t)$ and $I(0)$ are the luminescent intensity during the dacay and at $t = 0$, respectively. Here, s is a parameter to describe the distance dependence of the cross relaxation process. The values $s = 6$, 8 and 10, respectively, denote the electric dipole–dipole, dipole-quadrupole, and quadrupole-quadrupole interactions between luminescent centers. R_0 is the critical transfer distance, N is the concentration, τ_0 is the intrinsic radiation lifetime, and $\Gamma(1-(3/s))$ is a Gamma function. Here, $I(t)$ and I_0 are the luminescence intensity during the decay and $t = 0$ at room temperature, respectively. The fitted curves are shown in Fig. 7 as solid lines. The value of s derived from the fitting process is about 6.00. The results for t_0 from the data fitting with $s = 6$ are also summarized in Table 2. This indicates an energy transfer of elctric dipole–dipole interaction between Tb^{3+} and Yb^{3+}. The value of t_0 decreases rapidly with the increase of Yb^{3+} concentration in $LiYF_4$, implying a fast cross relaxation from Tb^{3+} to Yb^{3+} since the interaction of Yb^{3+} and Yb^{3+} changes from long to short distance.

The energy transfer efficiency (ETE) (η_{ETE}) and the total quantum efficiency (QE) (η_{QE}) can be determined from the luminescence decay curves. The energy transfer efficiency is defined as the ratio of Yb^{3+} ions depopulated by ET to Yb^{3+} ions over the total number of Tb^{3+} ions excited. η_{ETE} is obtained as a function of the Yb^{3+} concentration as the following [1], [17]:

$$\eta_{ETE} = \eta_{x\%Yb} = 1 - \frac{\int I_{x\%Yb}dt}{\int I_{0\%Yb}dt} \tag{4}$$

where I stands for the intensity of 544 nm at time t and $x\%$ Yb represents the Yb^{3+} concentration. Additionally, the relation between the energy transfer efficiency η_{ETE} and the quantum efficiency η_{QE} is linear and is defined as

$$\eta_{QE} = \eta_{Tb}(1-\eta_{ETE}) + 2\eta_{ETE} \tag{5}$$

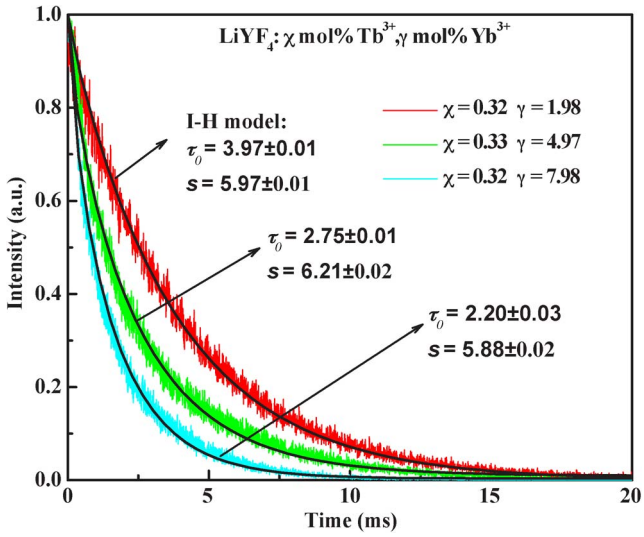

Fig. 7. Decay curves of the Tb^{3+}-Yb^{3+} ions co-doped LiYF[4] crystal samples surveyed at 544 nm under 486 nm excitation. The black solid lines are the I-H model fits for the decays.

where η_{QE} is the quantum efficiency for the Tb^{3+} ions. Ignoring the nonradiative energy loss by defects and impurities, the quantum efficiency for Tb^{3+} ions η_{Tb} is set to 1 [13], [21]. The values of the η_{ETE} and η_{QE} are also summarized in Table 2.

We can confirm from Table 2 that, when concentration of Yb^{3+} is held at ~1.97 mol%, the η_{ETE} reduces from 19.8% to 15.9% with the increase of Tb^{3+} concentration from 0.32 mol% to 1.05 mol%. And at the same 0.32 mol% Tb^{3+} concentration, the η_{ETE} increases monotonically from 19.8% to 66.7% with the increase of Yb^{3+} concentration from 1.98 mol% to 7.98 mol%. The maximum quantum efficiency value is 166.7% for 0.32 mol% Tb^{3+}/7.98 mol% Yb^{3+} co-doped $LiYF_4$ sample.

4. Conclusion

In summary, $LiYF_4$ samples doped with diverse Tb^{3+} and Yb^{3+} concentrations were synthesized by Bridgman method. Absorption, excitation and emission spectra study proved the occurrence of cooperative ET from Tb^{3+} to Yb^{3+} ions. With the excitation of Tb^{3+} ions by a blue photon at 486 nm, Yb^{3+} ions emit two NIR photons at 980 nm through cross relaxation ET from Tb^{3+} to Yb^{3+}, with maximum QE of as high as 166.7% for $LiYF_4 : Tb^{3+}$ (0.32 mol%)/Yb^{3+} (7.98 mol%) sample. Because of the advantages of efficient NIR QC and good chemical and optical properties, these $LiYF_4$ single crystals are promising materials for applications in solar cells.

References

[1] J. Hu, H. Xia, H. Hu, Y. Zhang, H. Jiang, and B. Chen, "Synthesis and efficient near-infrared quantum cutting of Pr^{3+}/Yb^{3+} codoped $LiYF_4$ single crystals," *J. Appl. Phys.*, vol. 112, no. 7, pp. 073518-1–073518-5, Oct. 2012.

[2] T. Trupke, M. A. Green, and P. Würfel, "Improving solar cell efficiencies by down-conversion of high-energy photons," *J. Appl. Phys.*, vol. 92, no. 3, pp. 1668–1674, Aug. 2002.

[3] C. Strümpel, M. McCann, G. Beaucarne, V. Arkhipov, A. Slaoui, V. Švrèek, C. del Cañizo, and I. Tobias, "Modifying the solar spectrum to enhance silicon solar cell efficiency—An overview of available materials," *Sol. Energy Mater. Sol. Cells*, vol. 91, no. 4, pp. 238–249, Feb. 2007.

[4] S. Kurtz and J. Geisz, "Multijunction solar cells for conversion of concentrated sunlight to electricity," *Opt. Exp.*, vol. 18, no. S1, pp. A73–A78, Apr. 2010.

[5] N. Tansu, J.-Y. Yeh, and L. J. Mawst, "Physics and characteristics of high performance 1200 nm InGaAs and 1300–1400 nm InGaAsN quantum well lasers obtained by metal–organic chemical vapour deposition," *J. Phys., Condens. Matter*, vol. 16, no. 31, pp. S3277–S3318, Aug. 2004.

[6] N. Tansu, J.-Y. Yeh, and L. J. Mawst, "High-performance 1200-nm InGaAs and 1300-nm InGaAsN quantum-well lasers by metalorganic chemical vapor deposition," *IEEE J. Sel. Topics Quantum Electron.*, vol. 9, no. 5, pp. 1220–1227, Sep./Oct. 2003.

[7] J. W. Ferguson, P. Blood, P. M. Smowton, H. Bae, T. Sarmiento, J. S. Harris, N. Tansu, and L. J. Mawst, "Optical gain in GaInNAs and GaInNAsSb quantum wells," *IEEE J. Quantum Electron.*, vol. 47, no. 6, pp. 870–877, Jun. 2011.
[8] L. Xu, D. Patel, C. S. Menoni, J.-Y. Yeh, L. J. Mawst, and N. Tansu, "Experimental evidence of the impact of nitrogen on carrier capture and escape times in InGaAsN/GaAs single quantum well," *IEEE Photon. J.*, vol. 4, no. 6, pp. 2262–2271, Dec. 2012.
[9] M. Wiemer, V. Sabnis, and H. Yuen, "43.5% efficient lattice matched solar cells," in *Proc. SPIE–Int. Soc. Opt. Eng.*, Sep. 2011, vol. 8108, pp. 810804-1–810804-5.
[10] R. M. Swanson, "Approaching the 29% limit efficiency of silicon solar cells," in *Conf. Rec. 31st IEEE Photovoltaic Spec. Conf.*, Jan. 2005, pp. 889–894.
[11] T. Trupke, M. Green, and P. Würfel, "Improving solar cell efficiencies by up-conversion of sub-band-gap light," *J. Appl. Phys.*, vol. 92, no. 7, pp. 4117–4122, Oct. 2002.
[12] Q. Y. Zhang, C. H. Yang, Z. H. Jiang, and X. H. Ji, "Concentration-dependent near-infrared quantum cutting in $GdBO_3 : Tb^{3+}$,Yb^{3+} nanophosphors," *Appl. Phys. Lett.*, vol. 90, no. 6, pp. 061914-1–061914-3, Feb. 2007.
[13] P. Vergeer, T. Vlugt, M. Kox, M. Hertog, J. Eerden, and A. Meijerink, "Quantum cutting by cooperative energy transfer in $Yb_xY_{1-x}PO_4 : Tb^{3+}$," *Phys. Rev. B, Condens. Matter*, vol. 71, no. 1, pp. 014119-1–014119-11, Jan. 2005.
[14] Q. Zhang, X. Liu, S. Ye, Z. Bin, Y. Qiao, G. Dong, B. Qian, D. Chen, Q. Zhou, and J. Qiu, "Cooperative quantum cutting in $Yb^{3+}-Tb^{3+}$ codoped borosilicate glasses," *IEEE Photon. Technol. Lett.*, vol. 21, no. 17, pp. 1169–1117, Sep. 2009.
[15] Q. Y. Zhang, G. F. Yang, and Z. H. Jiang, "Cooperative downconversion in $GdAl_3(BO_3)_4 : RE^{3+}$,Yb^{3+} (RE = Pr, Tb, and Tm)," *Appl. Phys. Lett.*, vol. 91, no. 5, pp. 051903-1–051903-3, Jul. 2007.
[16] G. Lakshminarayana and J. Qiu, "Near-infrared quantum cutting in RE^{3+}/Yb^{3+} (RE = Pr, Tb, and Tm):$GeO_2-B_2O_3-ZnO-LaF_3$ glasses via downconversion," *J. Alloy. Compd.*, vol. 481, no. 1/2, pp. 582–589, Jul. 2009.
[17] B. Xu, B. Yang, Y. Zhang, H. Xia, and J. Wang, "Cooperative energy transfer in Tm^{3+} and Yb^{3+} co-doped phosphate glasses," *J. Rare Earths*, vol. 31, no. 2, pp. 164–168, Feb. 2013.
[18] H. Zhang, J. Chen, and H. Guo, "Efficient near-infrared quantum cutting in $Ce^{3+} - Yb^{3+}$ co-doped YBO_3 phosphorsby," *J. Rare Earths*, vol. 29, no. 9, pp. 822–825, Sep. 2011.
[19] D. Chen, Y. Wang, Y. Yu, P. Huang, and F. Weng, "Quantum cutting downconversion by cooperative energy transfer from Ce^{3+} to Yb^{3+} in borate glasses," *J. Appl. Phys.*, vol. 104, no. 11, pp. 116105-1–116105-3, Dec. 2008.
[20] J. Sun, Y. Sun, and C. Cao, "Near-infrared luminescence and quantum cutting mechanism in CaWO4:Nd^{3+},Yb^{3+}," *Appl. Phys. B*, vol. 111, no. 3, pp. 367–371, May 2013.
[21] Q. Y. Zhang, C. H. Yang, and Y. X. Pan, "Cooperative quantum cutting in one-dimensional $(Yb_xGd_{1-x})Al_3(BO_3)_4 : Tb^{3+}$ nanorods," *Appl. Phys. Lett.*, vol. 90, no. 2, pp. 021107-1–021107-3, Jan. 2007.
[22] G. H. Beall and L. R. Pinckney, "Nanophase glass-ceramics," *J. Amer. Ceram. Soc.*, vol. 82, no. 1, pp. 1–16, Jan. 1999.
[23] Q. Wang, B. Yang, Y. Zhang, H. Xia, T. Zhao, and H. Jiang, "High light yield Ce^{3+}-doped dense scintillating glasses," *J. Alloy. Comp.*, vol. 581, pp. 801–804, Dec. 2013.
[24] B. Yang, Y. Zhang, B. Xu, F. Lai, H. Xia, and T. Zhao, "Scintillating properties of Ce^{3+}-doped high density oxide glasses," *Acta Phys. Sin.*, vol. 61, no. 19, p. 192 901, Mar. 2012.
[25] Q. Fang, H. Chen, F. Xu, S. Wang, Z. Liang, and C. Jiang, "Bridgman growth of $LiYF_4$ single crystal in nonvacuum atmosphere," *Chin. Opt. Lett.*, vol. 8, no. 11, pp. 1071–1174, Nov. 2010.
[26] S. Murakami, M. Herren, D. Rau, and M. Morita, "Photoluminescence and decay profiles of undoped and Fe^{3+}, Eu^{3+}-doped PLZT ceramics at low temperatures down to 10 k," *Inorg. Chim. Acta*, vol. 300–302, no. 20, pp. 1014–1021, Apr. 2000.
[27] J. K. Krebs and Z. J. Barninger, "Decay dynamics of Eu^{3+}/Tb^{3+} in solution-processed Y2O3," *J. Lumin.*, vol. 130, no. 7, pp. 1305–1307, Jul. 2010.
[28] J. Klafter and M. F. Shlesinger, "On the relationship among three theories of relaxation in disordered systems," *Proc. Nat. Acad. Sci. USA*, vol. 83, no. 4, pp. 848–851, Feb. 1986.